

Enhancement of hydrogen evolution reaction kinetics in alkaline media by fast galvanic displacement of nickel with rhodium – from smooth surfaces to electrodeposited nickel foams

Aleksandar Z. Jovanović^{1†}, Lazar Bijelić^{1†}, Ana S. Dobrota¹, Natalia V. Skorodumova², Slavko V. Mentus^{1,3}, Igor A. Pašti^{1,2*}

¹*University of Belgrade – Faculty of Physical Chemistry, Studentski trg 12-16, 11000 Belgrade, Serbia*

²*Department of Materials Science and Engineering, School of Industrial Engineering and Management, KTH – Royal Institute of Technology, Brinellvägen 23, 100 44 Stockholm, Sweden*

³*Serbian Academy of Sciences and Arts, Knez Mihajlova 35, 11000 Belgrade, Serbia*

† equally contributed

***Corresponding author:**

Dr. Igor Pašti

University of Belgrade – Faculty of Physical Chemistry

Studentski trg 12-16, 11158 Belgrade, Serbia

Email: igor@ffh.bg.ac.rs;

Abstract

Energy-efficient hydrogen production is one of the key factors for advancing the hydrogen-based economy. Alkaline water electrolysis is the main route for the production of high-purity hydrogen, but further improvements of hydrogen evolution reaction (HER) catalysts are still needed. Industrial alkaline electrolysis relies on Ni-based catalysts, and here we describe a drastic improvement of HER activity of Ni in alkaline media using several model catalysts for HER obtained upon nickel surface modification in aqueous solution of rhodium salts, when a spontaneous deposition of rhodium takes place based on the chemical displacement reaction $3\text{Ni} + 2\text{Rh}^{3+} = 3\text{Ni}^{2+} + 2\text{Rh}$. In the case of smooth Ni-poly electrodes, HER activity surpasses the activity of Pt-poly already after 30 s of exchange with Rh. SEM analysis showed that Rh is uniformly distributed, while surface roughness changes within 10%, agreeing with electrochemical measurements. Furthermore, XPS analysis has shown effective incorporation of Rh in the surface, while DFT calculations suggest that hydrogen binding is significantly weakened on the Rh-modified Ni surfaces. Such tuning of the hydrogen binding energy is seen as the main factor governing HER activity improvements. The same galvanic displacement protocols were employed for nickel foam electrodes and electrodeposited Ni on Ti mesh. In both cases, somewhat longer Rh exchange times are needed to obtain superior activities than for the smooth Ni surface, but up to 10 min. HER overpotential corresponding to -10 mA cm^{-2} for nickel foam and electrodeposited Ni electrodes, after modification with Rh, amounted to only -0.07 and -0.09 V , respectively. Thus, it is suggested that a fast spontaneous displacement of Ni with Rh could effectively boost HER in alkaline media with minor cost penalties compared to energy saving in the electrolysis process.

Keywords: alkaline water electrolysis; hydrogen production; modified Ni electrode; galvanic displacement; rhodium

1. Introduction

Faced with the global energy crisis, we strive to reduce fossil fuel consumption and increase the usage of renewable energy sources [1-3]. The electrochemical production of hydrogen *via* hydrogen evolution reaction (HER) is a promising way for obtaining clean and renewable energy [4]. In alkaline solutions the HER mechanism involves water dissociation and subsequent hydrogen reduction and adsorption ($\text{H}_2\text{O} + \text{e}^- \rightarrow \text{H}_{\text{ads}} + \text{OH}^-$), in the Volmer step, which is followed by, either the Heyrovsky step ($\text{H}_{\text{ads}} + \text{H}_2\text{O} + \text{e}^- \rightarrow \text{H}_2 + \text{OH}^-$) or by the Tafel step ($2\text{H}_{\text{ads}} \rightarrow \text{H}_2$) [5]. Recent improvements in the cost and performance of electrochemical water splitting technologies point towards a more economically viable future for their application at an industrial scale [6]. Currently, the two prevalent methods for obtaining hydrogen are proton-exchange membrane (PEM) electrolysis [7] and alkaline water electrolysis (AWE) [8]. The hydrogen production efficiency of PEM electrolyzers is higher but requires Pt-based catalysts [9]. In the case of AWE, the key goal is high catalytic activity and stability under intermittent polarization in alkaline media [10]. It is well known that the HER rate in alkaline media is inferior to that in acidic ones [11, 12] because of the additional water dissociation step [13], precedes the discharge step, but also due to the blockage of active sites by adsorbed hydroxyl ions, but also partly due to hydroxyl ion adsorption resulting in the blockage of active sites [5]. On the other hand, HER in alkaline media leads to less environmental pollution and equipment corrosion [4].

Nickel and nickel-based electrocatalysts have been thoroughly investigated because of nickel's excellent stability in alkaline media [14]. However, it has been shown that the catalytic activity of Ni largely depends on its morphology and active surface area [15, 16]. Therefore, multiple design strategies have been developed to increase the mediocre activity of clean Ni. Alloying Pt with Ni gives rise to two effects that increase the overall activity of the material. The first is the "ligand effect", referring to the change in electronic properties of both metals [17]. The other is the "lattice strain effect," which represents the change in Pt-Pt interatomic distance, resulting in a shift of the Pt *d*-band center [18]. A large number of non-PGM (PGM – platinum group metal) Ni alloys, such as binary and tertiary Ni-Mo alloys [20], NiCu [21], Raney Ni and NiCo [22], exhibit high activity.

Surface modification of Pt with Ni(OH)₂ is a prime example of a bifunctional electrocatalyst for alkaline HER. As suggested, Ni(OH)₂ promotes water dissociation, and the hydrogen intermediates subsequently adsorb and combine on the Pt surface [19], relying on tailoring catalytically active interfaces. Another approach for improving Ni performance is enhancing interfacial processes related to fast removing adsorbed hydrogen, like interfacing with reduced graphene oxide, which stimulated Hads spillover and improved HER activity [23] while maintaining excellent stability [24]. Despite numerous approaches to boost the HER activity of Ni, which work well in practice, a fundamental understanding of the key interactions in catalytic systems is of utmost importance.

It is well known that rhodium exhibits high catalytic activity towards both reduction and oxidation reactions [25]. Although several Rh-containing materials have been used in electrocatalysis of HER [26], only a small fraction of these was tested in alkaline media [27]. An example is a Ni₈₉Rh₁₁ alloy which has been experimentally shown to have excellent activity [28], which can largely be attributed to the bifunctionality of the surface. Furthermore, it was discussed that the Ni/Rh phases play the roles of H-adsorption/desorption sites, while the Ni(OH)₂ and Rh₂O₃ phases catalyze water dissociation, but no direct pieces of evidence were provided for such claims [28]. Moreover, Ni-Rh catalysts were also used for other catalytic reactions [29-32], showing the versatility of this catalytic system. However, the downside of Rh-containing catalysts is the high price of Rh, caused by its scarcity. With this in mind, it is important to optimize the design of novel Rh-containing electrocatalysts, taking advantage of the high catalytic activity of Rh while maintaining its low concentrations. Finally, it is important to note that the application of Ni/Rh electrocatalysts is potentially highly favorable, since not only does Rh enhance the HER performance [28, 33] and the overall water splitting [34], but, most likely, there is an underlying synergistic effect of Ni and Rh which could go beyond HER catalysis.

This study is aimed to investigate the effects of surface modification of Ni using galvanic displacement with Rh on the HER activity in alkaline media. Using the mentioned approach, only the surface of an electrocatalyst is modified with low amounts of Rh [35], which is highly beneficial for maintaining the low cost of such prepared catalysts while significantly increasing catalytic activity. The Rh-exchanged Ni electrodes, starting with smooth Ni surfaces to nickel foam and Ni

electrodeposits, were investigated by cyclic voltammetry for different duration of Ni immersion in rhodium salt solutions. In addition, the effects of electrode oxidation pretreatment were investigated to discuss the HER mechanism on modified electrodes. Apart from electrochemical measurements, the effects of the Rh-exchange process on the surface properties of Ni electrodes were also characterized by scanning electron microscopy with energy dispersive X-ray analysis (SEM/EDX) and X-ray photoelectron spectroscopy (XPS). Moreover, Density Functional Theory (DFT) calculations were used to rationalize the enhancement of HER activity upon surface modifications with Rh. We note that this work is focused on the origins of HER activity enhancement on various Ni surfaces upon spontaneous displacement with Rh, while the stability of investigated catalysts is not addressed.

2. Experimental

2.1. Surface Rh exchange and electrochemical measurements

Electrochemical measurements were done using IVIUM Vetex.One or Gamry Interface 1011e potentiostats in one compartment three-electrode electrochemical cell with Saturated Calomel Electrode (SCE) as a reference electrode and a 3×3 cm Ni foam (Goodfellow) as a counter electrode. As the electrolytic solution, 1 mol dm⁻³ KOH solution (Sigma Aldrich) prepared with ultrapure deionized water was used in all experiments. All the measurements were done at room temperature. In this work, potentials are referred to SCE, and to calculate overpotentials for HER, potentials are converted to the Reversible Hydrogen Electrode (RHE) scale as $E_{\text{RHE}} = E_{\text{SCE}} + 0.244 \text{ V} + 0.059 \text{ V} \times \text{pH}$ (pH = 13.45). Electrolyte resistance was corrected using hardware settings, but only up to 80 % of the resistance value, determined using single-point impedance measurement at -1 V vs. SCE. If a higher percentage of *iR* drop was corrected, the measurements were unstable. HER measurements were done using cyclic voltammetry at a sweep rate of 10 mV s⁻¹. Before the potential sweep, the electrode was held -1 V vs. SCE until current dropped below 1 μA cm⁻². No anodic excursions of the working electrode were allowed before the HER measurements unless explicitly stated otherwise.

2.1.1. Working electrodes preparation

The first set of measurements relates to smooth Ni-poly rotating disk electrodes (RDE). The Ni disk had a diameter of 3 mm and was inserted in a Teflon cylinder with a 10 mm diameter. The disk was polished to mirror-finish using alumina powder and then sonicated for 1 minute, washed in deionized water, diluted HCl, and again in deionized water. Then it was transferred to the electrolytic cell, and HER measurements were done. Ni/Rh displacement experiments were done by immersing Ni-poly RDE into 0.1 mol dm⁻³ RhCl₃ solution in 0.1 mol dm⁻³ HClO₄ for a given amount of time (for the measurements with Ni-poly RDE up to 45 s). After the exchange, the electrode was rinsed in deionized water, 1 mol dm⁻³ KOH solution, covered with the droplet of the same solution, and quickly transferred into the electrochemical cell. The transfer to the cell typically took under 30 s. During the HER measurements, the electrode was rotated at 1800 rpm to remove any bubbles formed on the surface, which could block the electrode surface.

The second set of the exchange and HER measurements was done using commercial nickel foam (NF) and electrodeposited Ni on Ti mesh (Special Metals, India) (Ni-dep). Before HER and Ni/Rh displacement experiments, NF (5×5 mm was exposed to the electrolyte) was cleaned in HCl, acetone, and deionized water. Exchange with Rh was done in the same way as for the Ni-poly disk. Then, HER measurements were done as described above. Ni-dep was produced on Ti mesh, previously cleaned in HCl, acetone, and deionized water. Ni deposition was done on Ti mesh with dimensions of 3×3 mm, from the deposition bath containing 0.2 mol dm⁻³ H₃BO₃, 0.5 mol dm⁻³ NH₄Cl, and 0.125 mol dm⁻³ NiSO₄. The deposition was done in a 2-electrode electrochemical cell, using Ni foam as a counter electrode, under potentiostatic conditions (2.4 V) for 90 s. Under these conditions, the typical deposition current is around 50 mA. Once the deposition was done, Ni-dep electrodes were thoroughly washed with deionized water and transferred to the electrochemical cell or Rh-exchange solution, the same one as described above.

We note that here we report currents normalized per geometric surface area. For the measurements with the Ni-poly disk, this is straightforward. For the measurements with NF, we used a geometrical cross-section multiplied by 2. The same is done for Ni-dep electrodes, but we excluded the surface of voids between the Ti wires forming the mesh. It is done because the used mesh is rather

sparse, and using a finer mesh would give higher currents within the same geometrical area (3×3 mm).

As a benchmark, we used a platinized Pt-poly disk (3 mm in diameter), prepared by potentiodynamic cycling of smooth Pt-poly disk in H_2PtCl_6 solution, as described in ref. [36]. Using H_{UPD} peaks, the roughness factor (RF) of the used platinized Pt-poly disk was evaluated to 7.9. In addition, the activity of the used Pt-disk was also checked in acidic media (0.5 mol dm^{-3} H_2SO_4 solution, **Figure S1**, Supplementary Information) using the same HER measurement protocol as in alkaline solution, confirming that a highly active Pt surface is obtained.

2.2. Characterization

Morphology analysis and chemical composition were probed using SEM-EDX with Phenom ProX Scanning Electron Microscope (Phenom, Netherlands). SEM characterization was done using an acceleration voltage of 10 kV, while the chemical composition was probed with the acceleration voltage of 15 kV.

XPS was used to assess the chemical speciation on the samples surfaces after the exchange with Rh. Samples were analyzed using SPECS Systems with XP50M X-ray source for Focus 500 and PHOIBOS 100/150 analyzer. $\text{AlK}\alpha$ source (1486.74 eV) at a 12.5 kV and 32 mA was used for this study. Survey spectra (0–1000 eV binding energy) were recorded with a constant pass energy of 40 eV, step size 0.5 eV and dwell time of 0.2s in the FAT mode. High-resolution spectra of Ni 2p and Rh 3d peaks were recorded with a constant pass energy of 20 eV, step size of 0.1 eV and dwell time of 2s in the FAT mode. Spectra were obtained at a pressure of 9×10^{-9} mbar. SPECS FG15/40 electron flood gun was used for charge neutralization to minimize the effects of charging at the samples. All the peak positions were referenced to C1s at 284.8 eV. Spectra were collected by SpecsLab data analysis software supplied by the manufacturer and analyzed with a commercial CasaXPS software package.

2.3. DFT calculations

The first-principle DFT calculations were performed using the Vienna ab initio simulation code (VASP) [37-39]. The Generalized Gradient Approximation (GGA) in the parametrization by

Perdew, Burk and Ernzerhof [40] combined with the projector augmented wave (PAW) method was used [41]. Cut-off energy of 600 eV and Gaussian smearing with a width of $\sigma = 0.025$ eV for the occupation of the electronic levels were used. A Monkhorst–Pack Γ -centered $14 \times 14 \times 1$ k-point mesh was used. We modelled Ni(001) and Ni(111) surfaces using the corresponding $p(2 \times 2)$ cells of given surfaces, with 10 and 9 layers slabs, respectively. Rh was inserted in the surface layer (Rh_{surf}) or the sub-surface layer (Rh_{sub}), and the top 6 layers of a given surface were allowed to relax fully. Knowing that on Ni HER proceeds under the conditions of high surface coverage [42], the surfaces were completely saturated by H_{ads} (1 monolayer of hydrogen, 4 H_{ads} per cell), and the average hydrogen binding energy ($E_{\text{H,b}}$) was calculated as:

$$E_{\text{H,b}} = (E_{\text{SURF+H}} - E_{\text{SURF}} - 4E_{\text{H}})/4 \quad (1)$$

where $E_{\text{SURF+H}}$, E_{SURF} , and $4E_{\text{H}}$ stand for the total energy of the surface with a monolayer of hydrogen, the total energy of the clean surface and the total energy of an isolated hydrogen atom. To convert $E_{\text{H,b}}$ to the Gibbs free energy for H_{ads} formation ($\Delta G_{\text{H,ads}}$), the procedure of Nørskov *et al.* [43] was used ($\Delta G_{\text{ads}}(\text{H}) = E_{\text{H,b}} + 1/2E_{\text{H}_2} + 0.24$ eV, E_{H_2} – the total energy of an isolated H_2 molecule).

3. Results and Discussion

3.1. Rh deposition – smooth Ni-poly surface

The clean, polished Rh disk measurements showed rather poor HER activity with η_{10} more negative than -0.4 V and the corresponding Tafel slope of -140 mV dec⁻¹ (**Figure 1**). Even though the Ni-poly disk was polished to a mirror finish, the roughness factor was somewhat higher than 1. By plotting the currents measured at -0.85 vs. SCE as the function of the potential scan rate and using the value of specific capacitance of 20 $\mu\text{F cm}^{-2}$ (for metallic surfaces [44, 45]), the roughness factor was determined to be 2.8. According to the benchmarking by McCrory *et al.* [46], η_{10} for the Ni surface with roughness factor 20 ± 10 was approximately -0.25 V. For the exchange with Rh up to 20 s, we could not see any significant changes in recorded cyclic voltammograms (**Figure S2**, Supplementary Information), but obtained a significant increase of HER activity. However, for 30 s of exchange with Rh and more, cyclic voltammetry of Rh-exchanged Ni-poly disk shows H_{UPD} regions characteristic for Rh [47] and practically unchanged regions corresponding to $\text{Ni}^{2+}/\text{Ni}^{3+}$ oxidation (**Figure 1**). For 15,

30, and 45 s of exchange with Rh, η_{10} amounted to -168 , -120 , and -110 mV, without significant change of the Tafel slope. These results align with the unchanged surface roughness, evidenced by 3D surface reconstruction using SEM, and a low percentage of Rh on the surface for short Rh-exchange times, with a very uniform distribution. These issues will be discussed later on.

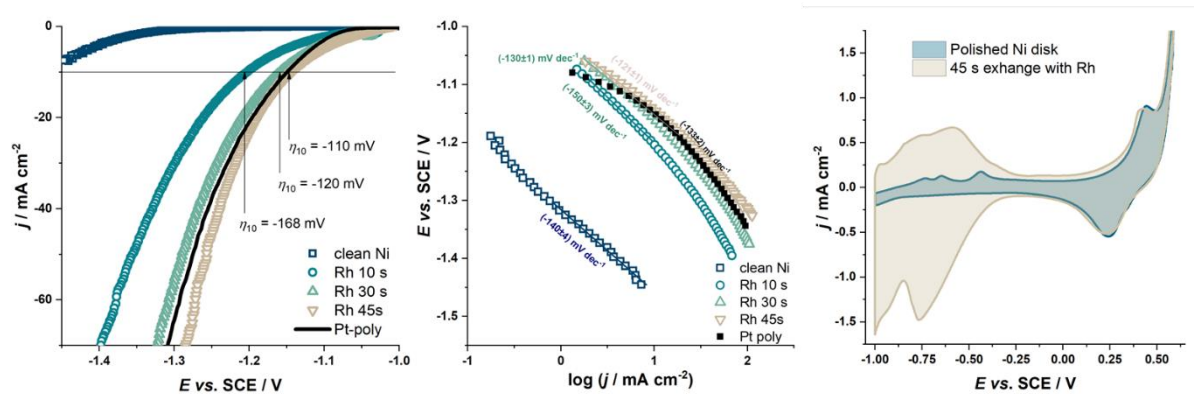


Figure 1. HER activity measurements on Rh-exchanged smooth Ni-poly: Ni HER polarization curves of smooth Ni-poly disk before and after 10 s, 30 s, and 45 s of exchange with Rh. A solid black line gives the HER polarization curve of the platinized Pt-poly disk (left) and the corresponding Tafel plots (middle). On the right, the cyclic voltammogram of smooth Ni-poly disk is compared to the cyclic voltammogram of Ni-poly disk after 45 s of exchange with Rh at a potential sweep rate of 10 mV s^{-1} .

We have used platinized Pt-poly as a reference to Rh-modified Ni-poly surfaces. In ref. [46] η_{10} for Pt was reported to amount (-100 ± 20) mV for smooth Pt-poly surface (RF 6 ± 2), and ~ -40 mV for Pt-poly with RF of 90 ± 20 . Our Pt disk has η_{10} of -110 mV, which closely agrees with the results of McCrory *et al.* [46]. Given that the RF values of Ni-poly do not change for more than 10% upon the exchange with Rh (**Figures S2** and **S3**, Supplementary Information), and that the Rh-exchanged electrodes have measured HER current densities (normalized per geometric surface area) close to that of Pt (**Figure 1**), surface-specific activities of Rh-exchanged Ni-poly actually exceed the activities of Pt (**Figure 2**).

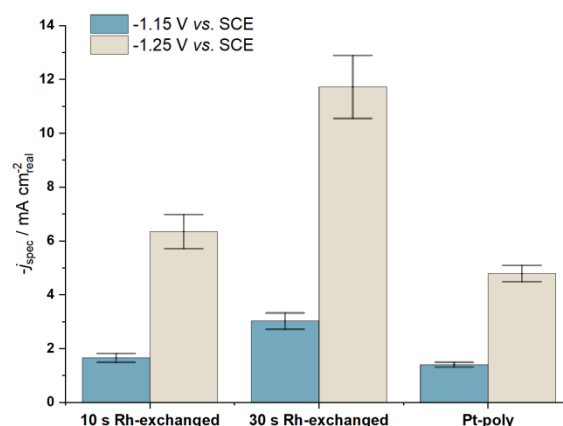


Figure 2. Surface specific activities (determined as current densities divided by the corresponding roughness factors) for 10 s and 30 s Rh-exchanged Ni-poly and platinized Pt-poly disk electrodes at two different potentials.

A direct comparison with the results of Nguyen *et al.* [33], who investigated HER activity of NiRh₃ alloy nanosponges in alkaline media, can be made. With the catalyst loading of 169 $\mu\text{g cm}^{-2}$, the authors reported η_{10} of -107 mV for NiRh₃ alloy and -119 mV for commercial Pt/C catalyst [33]. The previous improvements of HER activity were achieved using similar approaches, like spontaneous deposition of Pd and Rh on smooth Pt-poly (RF 2) [48], where Rh-modified Pt-poly showed higher HER activity than Pd-modified Pt-poly, without significant change of the roughness factor (2.1 for Rh-modified surface, and 2.08 for Pd-modified surface). Described catalytic surfaces should also be compared to pure Rh, and recently Rh films on Ni foam and Ti mesh, prepared by aerosol-assisted chemical vapor deposition (AACVD) technique, were investigated as HER catalysts in alkaline media [49]. It was found that Rh film on NF had η_{10} of -127 mV, while the one prepared on Ni mesh had the corresponding overvoltage of -67 mV [49]. As there are many studies of HER catalysts in alkaline media, it would be possible to extend the comparison with literature data to a large number of reports. However, here we refer to the review of Bouzek *et al.* [7], who provided an extensive summary of literature reports. The assembled HER activities in the mentioned work classify Rh-modified Ni into the first 25% of highly active Pt-free HER catalysts in alkaline media.

The examples of SEM analyses with EDX mapping (**Figure 3**) show uniform distributions of Rh and O on the Ni-poly surface exchanged with Rh. Surface reconstruction profiles show surface roughness variations below 10% with (see also **Figure S3**, Supplementary Information) typical height

variations along the surface of 100 nm over 25×25 μm surface snapshots. Minor variations of surface roughness during the exchange with Rh also agree with the cyclic voltammetry of exchanged Ni-poly electrodes (**Figure S2**, Supplementary Information). XPS measurements (**Figure 3**, lower panel) indicate the presence of metallic Ni, Ni(OH)₂ and NiRh_x phase (from Ni 2p high-resolution spectra) and Rh³⁺ and metallic Rh (from Ni 3d high-resolution spectra) [33, 50, 51]. The results shown are for 10 s exchange with Rh, in which case neither electrochemistry nor SEM shows the formation of well-defined Rh islands, but it is obvious that there are certain parts of the surface containing Rh aggregates. However, after 30 s exchange with Rh, there are clear indications that Rh islands are formed, and the effect is more prominent for higher exchange times. For example, after 45 s of exchange with Rh, the characteristic H_{UPD} region is clearly seen (**Figure 1**), which is the feature of the Rh phase [47]. This observation unambiguously confirms that longer exchange times lead to the formation of metallic Rh islands on the Ni-poly surface.

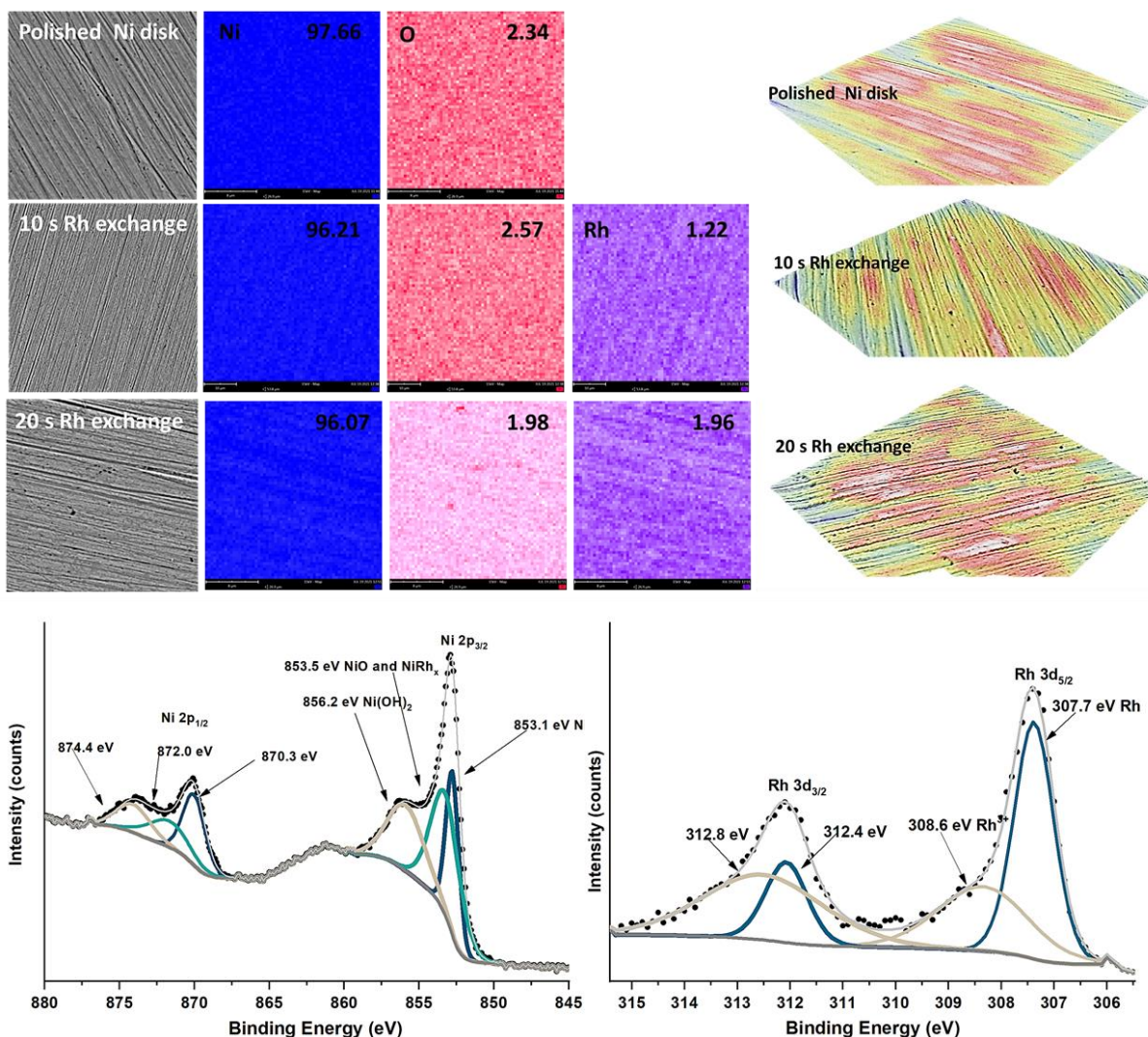


Figure 3. SEM+EDX and XPS characterization of Ni surface upon exchange with Rh. Top left SEM images and EDX elemental maps of Ni, O, and Rh are shown, along with the atomic percentage of each element. The top right is the corresponding 3D SEM surface reconstruction (before and after 10 and 20 s of exchange with Rh, respectively). On the bottom, de-convoluted high-resolution XPS signals of Ni 2p and Rh 3d are given (10 s exchange with Rh).

3.2. HER mechanism on Rh-modified Ni surfaces

In order to rationalize enhanced HER activity of Rh-exchanged Ni surface, we turned to the analysis of H_{ads} energetics on Rh-modified Ni surfaces. We studied Ni(111) and Ni(001) using DFT calculations, and to model modification by Rh, we added Rh in the surface or subsurface layer of these Ni(hkl), effectively modelling the surface of subsurface alloys. We find that surface incorporation of Rh is energetically more favored than subsurface inclusion of Rh on both Ni surfaces, in agreement with previous reports [52]. In the case of Ni(111), surface incorporation of Rh

is more favored by -0.20 eV, while this difference for Ni(001) is -0.11 eV. Considering that H_{ads} energetics was shown to give the volcano-type relationship with HER activities in alkaline media [53], just like in acidic media [54], we used the methodology of Nørskov *et al.* [43] to establish activity trends. The results show that surface modification of Ni(111) and Ni(001) by Rh incorporation significantly reduced H_{ads} energetics compared to pristine Ni(111) and Ni(001), thus reducing the energy required for the formation of H_2 from H_{ads} (**Figure 4**). This effect is due to the modification of the Ni electronic structure due to the presence of Rh atoms. It is seen even when Rh is incorporated in the subsurface of Ni(111) and Ni(001) (**Figure 4**). We do not engage here in a detailed analysis of the origin of altered H_{ads} energetics on modified Ni surface, which would involve the analysis of the stabilization of the d-band center of Ni by Rh. However, we note that Ni-Rh surface alloy (Ni host, Rh solute) was previously identified to have favorable H_{ads} energetic for HER ($|\Delta G_{\text{ads}}(\text{H})| < 0.1$ eV) by Greeley *et al.* [55], for higher surface concentrations of Rh (1/3 of monolayer), but such catalyst was not implemented experimentally.

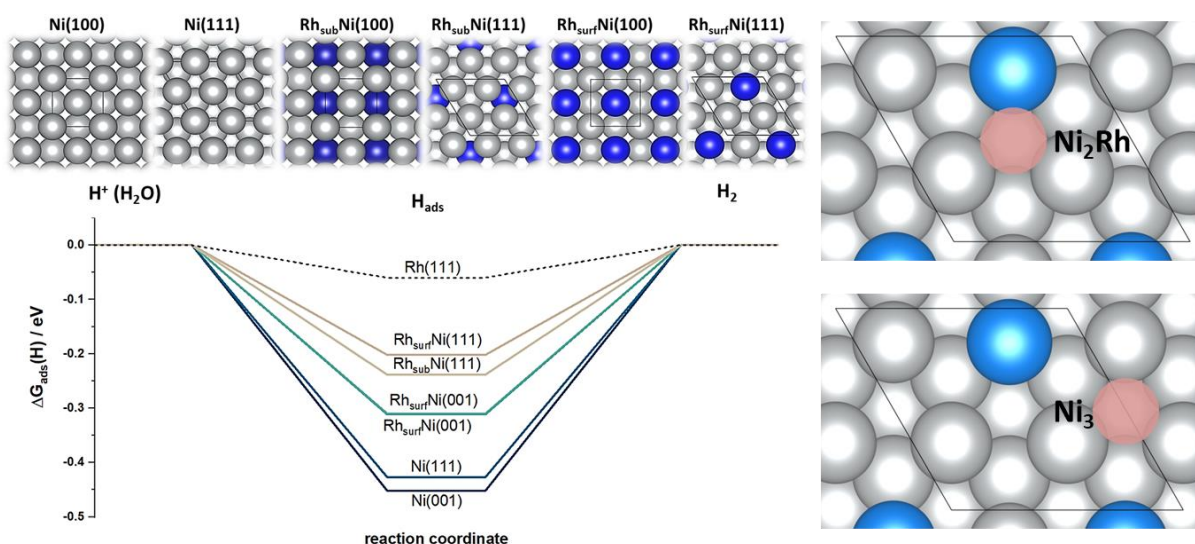


Figure 4. Enhancement of HER activity of Rh-exchanged Ni surfaces according to theoretical calculations. The upper panel shows the model surfaces studied here with Rh atoms incorporated in the surface (Rh_{surf}) or the subsurface layer (Rh_{sub}). The lower panel shows $\Delta G_{\text{ads}}(\text{H})$ profiles for studied surfaces, demonstrating that adjusted H_{ads} formation energetics should enhance HER activity. On the right, two inequivalent fcc sites on $\text{Rh}_{\text{surf}}\text{Ni}(111)$ are shown, marked as Ni_2Rh site and Ni_3 site.

Tafel analysis performed on HER polarization curves of Rh-exchanged smooth Ni-poly shows Tafel slopes that are close but usually larger than -120 mV dec^{-1} (absolute values). Deviation from the theoretical value of -120 mV dec^{-1} can be ascribed to incomplete correction for the iR drop (see Section 2.1) and the problems with removing H_2 bubbles (despite electrode rotation during the measurements). Thus, although there it is quite inconvincible to determine the mechanism of HER solely based on the Tafel slope, there is enough reliable literature data [42] to conclude that Heyrovski reaction is the rate-determining step (RDS) on Ni-poly surface, at least at higher HER overpotentials where we performed Tafel analysis. The same reference claims that, at lower HER overpotentials, the Tafel reaction is the RDS [42]. However, more recent findings suggest that surface modifications by Ni-oxy-hydroxides enhance HER kinetics through H_2O dissociation where H_{ads} ends up on the metal surface. At the same time, OH_{ads} is governed by the oxy-hydroxide phase (and ultimately released back to the solution) [19, 56]. In the original interpretation, this means that the rate of Volmer reaction is increased, allowing fast recombination of H_{ads} and formation of molecular H_2 *via* the Tafel step. Thus, if the Ni surface is partially oxidized, HER activity should increase, and this is exactly what we observe for clean Ni-poly (**Figure 4**), while the Tafel slope changes from -140 mV dec^{-1} for clean Ni-poly to -90 mV dec^{-1} for oxidized Ni-poly. This change of the Tafel slope is insufficient to claim any change of the reaction mechanism unambiguously but might be a good indication of such a scenario. Namely, the Heyrovsky reaction also involves H_2O dissociation, and if the H_2O dissociation rate is increased, one can also expect that HER proceeds through with the Heyrovsky reaction as the RDS will be enhanced. Actually, the Ni surface binds H_{ads} strongly, so there is no reason to expect that the Volmer reaction (formation of H_{ads}) will be RDS, in agreement with ref. [42]. Nevertheless, the HER activity significantly decreases if the Rh-exchanged surface is exposed to the same oxidation protocol (**Figure 4**). Rh surface binds H_{ads} weaker than Ni surface, but, still, $\Delta G_{\text{ads}}(\text{H})$ is negative (**Figure 4**). However, the Rh|Ni interface conversion to Rh|Ni-oxy-hydroxide interface hinders HER. As Rh-exchanged Ni surface binds H_{ads} weaker than clean Ni surface, there is no reason to expect that Ni-oxy-hydroxide surface will bind OH_{ads} weaker than on pure Ni surface, Brønsted–Evans–Polanyi relations for water dissociation [57] suggest lower H_2O dissociation rate. Thus, slower Volmer and Heyrovsky reactions compared to pure Ni surface. However, on pure Ni-poly Tafel reaction is the

RDS at low overpotentials due to strong binding of H_{ads} , but this is not the case for Rh-exchanged surface, and the surface is effectively cleaned from H_{ads} by fast recombination/desorption and the formation of molecular H_2 . However, we also observed an additional effect of surface oxidation. For clean Ni surface, activity increases as the oxidation time increases from 10 to 30 s. However, for Rh-modified Ni surface, the effect is the opposite. The HER activity slightly decreases with the elongation of the oxidation time. It could mean that the mechanism of HER on Rh-modified surface is still Volmer-Heyrovsky, like in the case of pure Ni surface, but the oxidation causes the blockage of the active sites for the formation of H_{ads} , effectively lowering HER activity. Moreover, the negative effect of the surface oxidation could also be a clear indication that the surface oxide phase of Rh-modified Ni surface is less active for water dissociation than oxidized Ni surface and that pure Ni-Rh surface actually provides better energetics for water dissociation. In contrast, the opposite holds for the clean Ni surface. Overall, our results suggest synergistic action of Ni and Rh and that the explanations of HER activity based on H_{ads} accepting sites (Rh site) and OH accepting sites (oxy/hydroxide sites) [28] should be reexamined. This conclusion is supported by the fact that for 0.25 ML H_{ads} on studied Rh_{surf} -Ni(111), DFT calculations point to a very low variation of hydrogen binding energy on Ni_3 sites (-2.71 eV) and Ni_2Rh sites (-2.75 eV), suggesting that the surface is energetically quite uniform, while it is obvious that the clean Rh phase prefers H_{ads} less than Ni phase (Figure 4).

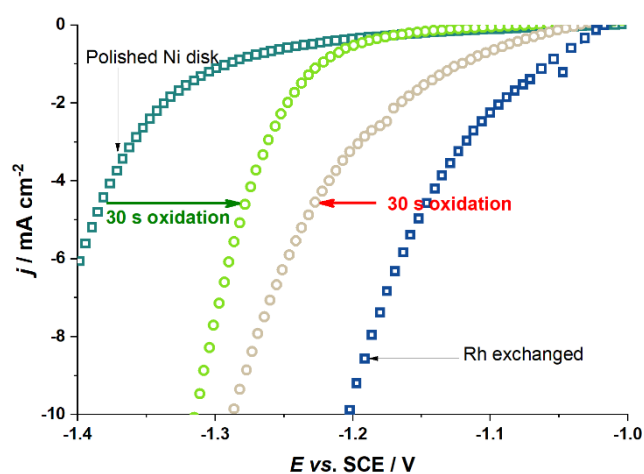


Figure 5. The comparison of HER activities after exposure of smooth Ni-poly and Rh-exchanged Ni-poly disk (20 s of exchange) to anodic polarization at 0 V vs. SCE for 30 s. Before recording HER polarization curves, electrodes were held at -1 V vs. SCE, as explained in Section 2.1.

3.3. Rh exchange on expanded Ni surfaces

While metallic Rh is extremely expensive [58], significant improvements of HER activity of Rh-exchanged Ni, surpassing the activity of Pt (**Figure 3**), suggest this approach could be effectively used for boosting commercially available Ni-based HER catalyst for alkaline water electrolysis. In fact, a rough estimate based on the surface density of Ni(001) surface shows that replacing a full monolayer of Ni atoms with Rh atoms would cost only ~ 1.4 \$ *per* m^2 of Ni (the real surface area). Considering tremendous HER activity improvement, this is a small cost compared to the energy savings achievable using described surface modification of Ni. Thus, we further explore the effects of Rh exchange on the HER activity of extended Ni surface.

First, we investigate the effect of Rh exchange on commercial Ni foam. The results show that the effects of time of exchange by Rh are not as pronounced as in the case of smooth Ni surface (**Figure 6**), and the most pronounced effects are seen after several minutes of exchange by Rh. For clean NF η_{10} was found to be -0.26 V, and for 2 and 10 min exchange with Rh it reduces to -0.17 , and -0.07 V. EDX analysis showed a monotonous increase of Rh surface concentration, without significant alteration of mesh morphology caused by dissolution in acidic Rh-containing solution (**Figure 6**). Nevertheless, for higher Rh exchange times, we clearly observed the formation of Rh phase on NF surface (**Figure S4**, Supplementary Information), which we consider mainly responsible for HER activity, as metallic Rh is much more active for HER than Ni. Also, we must note that it was impossible to perform electrode rotation to remove the H_2 bubbles formed on the surface in the case of NF. Thus the measured activity of Rh-exchanged Ni foam is slightly affected by H_2 bubbles blocking the surface. Still, the activities are better than those reported for pure Rh films prepared on NF using AACVD [49], while the modification procedure is greatly simplified. We also note that the improvements of the NF HER activity were previously reported for the case of spontaneous deposition of Ru and Pd [59]. However, the activities reported in that work are much lower than those reported here, not only for the modified NF but also for the clean one.

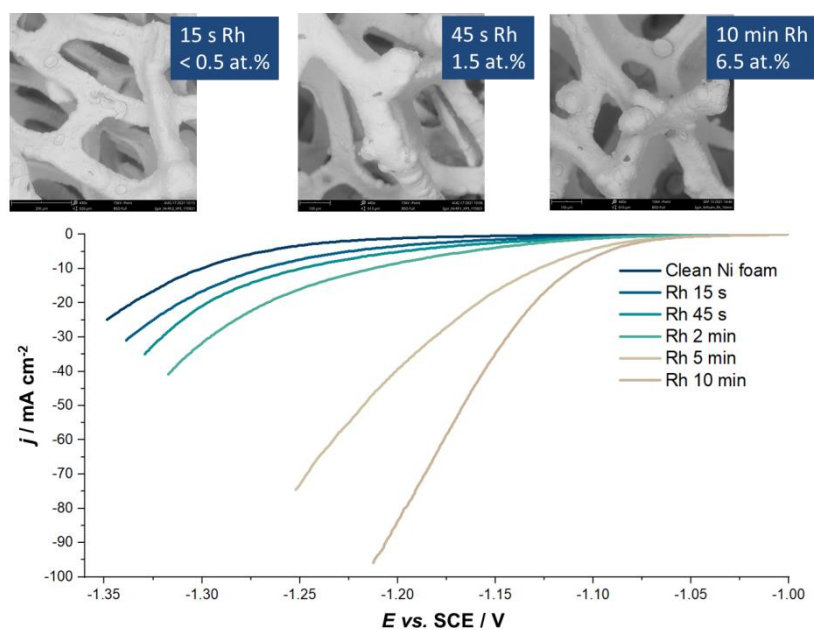


Figure 6. Improvement of HER activity of commercial NF upon exchange with Rh, from 15 s to 10 min, with insets showing SEM images and EDX results concerning Rh concentration.

Next, we also investigated the improvement of HER *via* Rh-exchange of electrodeposited Ni electrodes on Ti mesh (Ni-dep electrodes). The improvement of HER is undoubtedly seen (**Figure 7**). Under the used Ni deposition conditions, there is an intense H₂ evolution. Thus, the surface of Ni-dep electrodes is highly developed through H₂-bubble templating [60], while 15±2 μm thick Ni deposits are obtained (**Figure S5**, Supplementary Information), growing in dendritic form. For as-deposited Ni-dep electrodes, η_{10} amounts to -0.29 V. Based on the voltammetric peaks corresponding to Ni²⁺/Ni³⁺ (**Figure 7**, top right) and the corresponding voltammetric responses of smooth Ni-poly (**Figure S2**, Supplementary Information), roughness factor is estimated to be 50±10. Similar to the case of commercial NF, the effects of Rh exchange are not as pronounced as for smooth Ni-poly but are more than clear. For 30 s of exchange by Rh, η_{10} is reduced to -0.15 V. SEM images taken at the identical location before and after the exchange procedure (**Figure S6**, Supplementary Information) show no significant changes of Ni-dep morphology. More interestingly, EDX showed no Rh (thus, Rh concentration was below < 0.005 at.%), but HER activity was visibly enhanced. Considering the results obtained with NF and Ni-dep electrodes, compared to the ones with smooth Ni-poly, we

believe that in the case of highly developed Ni surfaces, Rh exchange is hindered by diffusion of Rh-containing solution through such highly-developed surfaces.

For this reason, we also investigated long Rh exchange time, 5 minutes, and obtained a further improvement of HER activity. In this case, η_{10} amounted to -0.09 V, and the Tafel slope was -122 ± 5 mV dec⁻¹. However, after SEM and EDX analysis, it was observed that the surface is significantly eroded (**Figure S7**, Supplementary Information), while EDX showed ~ 20 at.% Rh, in line with clear H_{UPD} peaks after 5 min of exchange with Rh (**Figure 7**). This finding is in line with recorded cyclic voltammograms of Ni-dep electrodes before and after Rh exchange, showing progressive loss of voltammetric response corresponding to Ni^{2+}/Ni^{3+} transition with the extension of Rh exchange time (**Figure 7**). Such erosion of Ni-dep is likely due to fast corrosion of a highly developed Ni surface, and it was not observed for NF or smooth Ni-poly. We ascribe this to the fact that Ni-poly has a low concentration of highly uncoordinated Ni sites, prone to corrosion, unlike Ni-dep. Moreover, the surface of NF is also rather smooth, much smoother than that of Ni-dep (**Figure 6**, insets, and **Figure 7**). We believe this is why no pronounced dissolution and erosion of NF is seen.

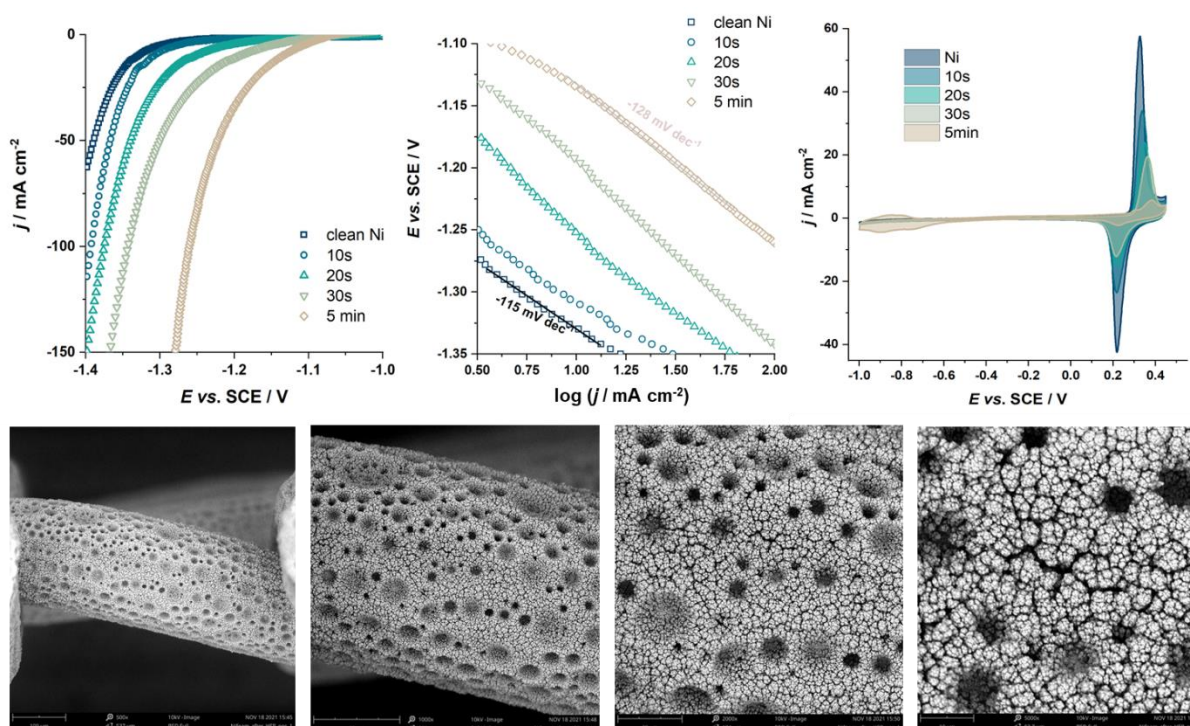


Figure 7. Enhancement of HER on Ni-dep electrodes. The upper panel shows the HER currents of as-deposited Ni-dep electrode and after the exchange with Rh for 10 s, 20 s, 30 s, and 5 min (top left), corresponding Tafel plots (top middle), and the cyclic voltammograms (common potential sweep rate

of 100 mV s^{-1} , top right). The lower panel shows the SEM images of the Ni-dep electrode at different magnifications.

4. Conclusions

Fast galvanic exchange of Ni with Rh, using concentrated acidic Rh solution, leads to tremendous HER activity improvements in alkaline media. In the case of a smooth Ni-poly surface, HER activity surpasses Pt-poly for Rh exchange times of 30 seconds. Our results suggest that there is no significant change in the surface roughness of Rh-exchanged electrodes, and when surface-specific activities of Rh-exchanged smooth Ni-poly are compared to that of Pt-poly, the HER activity of the modified Ni-poly (30 s of exchange) is roughly 2.5 times higher than the activity of Pt-poly. DFT calculations suggest that Rh-modified Ni surface interacts weaker with H_{ads} , making the formation of H_2 easier. Based on the obtained result, we suggest that the mechanism of HER in alkaline media is the same for Ni-poly and Rh-modified Ni-poly. More precisely, at high HER overpotentials, the HER proceeds through the Volmer-Heyrovsky mechanism, and the activity enhancement is through a synergistic effect of Ni and Rh, which provides suitable energetics for water dissociation and removal of H_{ads} . This conclusion is justified by the negative effects of surface oxidation on the HER activity of Rh-modified Ni surface. Further, we employed the same Rh exchange protocols for highly developed Ni electrodes – commercial Ni foam and electrodeposited Ni on Ti mesh. In both cases, HER was improved, but longer exchange times are needed to observe improvements similar to the smooth Ni-poly. For example, after 10 minutes of exchange using commercial NF, HER overpotential (η_{10}) is reduced down to -0.07 V . No pronounced corrosion is seen, but the surface Rh phase was observed using SEM. Likewise, for electrodeposited Ni electrodes, after 5 minutes of exchange with Rh, η_{10} amounted -0.09 V . However, in this case, the Ni-dep electrode was significantly eroded due to pronounced corrosion in acidic media. Despite the extremely high price of Rh, surpassing the price of Pt by a factor of 15, it can be estimated that the complete replacement of the surface layer of Ni with Rh increases the price of the catalyst by roughly $1.4 \text{ \$ per m}^2$ of Ni surface. Thus, rapid galvanic displacement of Ni by Rh could be a suitable route for enhancing HER activity of high-surface area Ni-based catalysts for alkaline electrolysis, even at the industrial scale.

Acknowledgment

This research was funded by the Science Fund of the Republic of Serbia (PROMIS project RatioCAT), Ministry of Education, Science, and Technological Development of the Republic of Serbia (Contract No. 451-03-68/2020-14/200146), and Swedish Research Council (grant no 2019-05580). S.V.M. and I.A.P. are indebted to the Research Fund of the Serbian Academy of Sciences and Arts, project F-190, for supporting this study. The computations and data handling were enabled by resources provided by the Swedish National Infrastructure for Computing (SNIC) at the National Supercomputer Centre (NSC) at Linköping University, partially funded by the Swedish Research Council through grant agreement No. 2018-05973.

References

- [1] J. A. Turner, Sustainable hydrogen production. *Science* **305**, 972–974 (2004). DOI: 10.1126/science.1103197
- [2] S. Chu, A. Majumdar, Opportunities and challenges for a sustainable energy future. *Nature* **488**, 294–303 (2012). DOI: 10.1038/nature11475
- [3] N. S. Lewis, D. G. Nocera, Powering the planet: Chemical challenges in solar energy utilization. *Proc. Natl. Acad. Sci. U.S.A.* **103**, 15729–15735 (2006). DOI: 10.1073/pnas.0603395103
- [4] L. Tang, J. Yu, Y. Zhang, Z. Tang, Y. Qin. Boosting the hydrogen evolution reaction activity of Ru in alkaline and neutral media by accelerating water dissociation. *RSC Adv.* **11**, 6107-6133 (2021). <https://doi.org/10.1039/D0RA09515J>
- [5] N. M. Markovic, P. N. Ross Jr., Surface science studies of model fuel cell electrocatalysts. *Surface Science Reports* **45**, 117-229 (2002) [https://doi.org/10.1016/S0167-5729\(01\)00022-X](https://doi.org/10.1016/S0167-5729(01)00022-X)
- [6] I. Staffell, D. Scamman, A. V. Abad, P. Balcombe, Paul. E. Dodds, P. Ekins, N. Shah, K. R. Ward, The role of hydrogen and fuel cells in the global energy system. *Energy Environ. Sci.* **12**, 463-491 (2019) DOI: 10.1039/C8EE01157E

- [7] M. Durovic, J. Hnat, K. Bouzek, Electrocatalysts for the hydrogen evolution reaction in alkaline and neutral media. A comparative review. *Journal of Power Sources* **493**, 229708 (2021) <https://doi.org/10.1016/j.jpowsour.2021.229708>
- [8] D. Pletcher, X. Li, Prospects for alkaline zero gap water electrolyzers for hydrogen production. *International Journal of Hydrogen Energy* **36**, 15089-15104 (2011) <https://doi.org/10.1016/j.ijhydene.2011.08.080>
- [9] A. Eftekhari, Electrocatalysts for hydrogen evolution reaction. *International Journal of Hydrogen Energy* **42**, 11053-11077 (2017) <https://doi.org/10.1016/j.ijhydene.2017.02.125>
- [10] F. Safizadeh, E. Ghali, G. Houlachi, Electrocatalysis developments for hydrogen evolution reaction in alkaline solutions – A Review. *International Journal of Hydrogen Energy* **40**, 256-274 (2015) <https://doi.org/10.1016/j.ijhydene.2014.10.109>
- [11] J. Durst, A. Siebel, C. Simon, F. Hasche, J. Herranz, H. A. Gasteiger, New insights into the electrochemical hydrogen oxidation and evolution reaction mechanism. *Energy & Environmental Science* **7**, 2255-2260 (2014) DOI: [10.1039/C4EE00440J](https://doi.org/10.1039/C4EE00440J)
- [12] J. Durst, C. Simon, A. Siebel, P. Rheinländer, T. Schuler, M. Hanzlik, J. Herranz, F. Hasché, H. A. Gasteiger, Hydrogen Oxidation and Evolution Reaction (HOR/HER) on Pt Electrodes in Acid vs. Alkaline Electrolytes: Mechanism, Activity and Particle Size Effects. *ECS Transactions* **64**, 1069-1080 (2014) DOI: [10.1149/06403.1069ecst](https://doi.org/10.1149/06403.1069ecst)
- [13] Y. Zheng, Y. Jiao, Y. Zhu, L. H. Li, Y. Han, Y. Chen, M. Jaroniec, S. Z. Qiao, High electrocatalytic hydrogen evolution activity of an anomalous ruthenium catalyst. *Journal of the American Chemical Society* **138**, 16174-16181 (2016) <https://doi.org/10.1021/jacs.6b11291>
- [14] X. Hu, X. Tian, Y. W. Lin, Z. Wang, Nickel foam and stainless steel mesh as electrocatalysts for hydrogen evolution reaction, oxygen evolution reaction and overall water splitting in alkaline media. *RSC Advances* **9**, 31563-31571 (2019) <https://doi.org/10.1039/C9RA07258F>
- [15] M. A. McArthur, L. Jorge, S. Coulombe, S. Omanovic, Synthesis and characterization of 3D Ni nanoparticle/carbon nanotube cathodes for hydrogen evolution in alkaline electrolyte. *Journal of Power Sources* **266**, 365-373 (2014) <https://doi.org/10.1016/j.jpowsour.2014.05.036>

- [16] S. H. Ahn, S. J. Hwang, S. J. Yoo, I. Choi, H. J. Kim, J. H. Jang, S. W. Nam, T. H. Lim, T. Lim, S. K. Kim, J. J. Kim, Electrodeposited Ni dendrites with high activity and durability for hydrogen evolution reaction in alkaline water electrolysis. *Journal of Materials Chemistry* **22**, 15153-15159 (2012) <https://doi.org/10.1039/C2JM31439H>
- [17] J. R. Kitchin, J. K. Norskov, M. A. Barteau, J. G. Chen, Modification of the surface electronic and chemical properties of Pt(111) by subsurface 3d transition metals. *Journal of Chemical Physics* **120**, 10240 (2004) DOI: 10.1063/1.1737365
- [18] Q. Jia, W. Liang, M. K. Bates, P. Mani, W. Lee, S. Mukerjee, Activity Descriptor Identification for Oxygen Reduction on Platinum-Based Bimetallic Nanoparticles: *In Situ* Observation of the Linear Composition–Strain–Activity Relationship. *ACS Nano* **9**, 387-400 (2015) <https://doi.org/10.1021/nn506721f>
- [19] R. Subbaraman, D. Tripkovic, K. C. Chang, D. Strmcnik, A. P. Paulikas, P. Hirunsit, M. Chan, J. P. Greeley, V. R. Stamenkovic, N. M. Markovic, Trends in activity for the water electrolyser reactions on 3d M(Ni,Co,Fe,Mn) hydr(oxy)oxide catalysts. *Nat. Mater.* **11**, 550 – 557 (2012) DOI: [10.1038/nmat3313](https://doi.org/10.1038/nmat3313)
- [20] I. A. Raj, K. I. Vasu, Transition metal-based hydrogen electrodes in alkaline solution — electrocatalysis on nickel based binary alloy coatings. *Journal of Applied Electrochemistry*, **20**, 32-38 (1990) <https://doi.org/10.1007/BF01012468>
- [21] R. Solmaz, A. Doner, G. Kardas, The stability of hydrogen evolution activity and corrosion behavior of NiCu coatings with long-term electrolysis in alkaline solution. *International Journal of Hydrogen Energy* **34**, 2089-2094 (2009) <https://doi.org/10.1016/j.ijhydene.2009.01.007>
- [22] I. Herraiz-Cardona, C. Gonzalez-Buch, C. Valero-Vidal, E. Ortega, V. Perez-Herranz, Co-modification of Ni-based type Raney electrodeposits for hydrogen evolution reaction in alkaline media. *Journal of Power Sources* **240**, 698-704 (2013) <https://doi.org/10.1016/j.jpowsour.2013.05.041>
- [23] S. J. Gutic, A. S. Dobrota, M. Leetmaa, N. V. Skorodumova, S. V. Mentus, I. A. Pasti, Improved catalysts for hydrogen evolution reaction in alkaline solutions through the electrochemical formation

of nickel-reduced graphene oxide interface. *PCCP* **19**, 13281-13293 (2017)

<https://doi.org/10.1039/C7CP01237C>

[24] D. Chanda, J. Hnat, A. S. Dobrota, I. A. Pasti, M. Paidar, K. Bouzek, The effect of surface modification by reduced graphene oxide on the electrocatalytic activity of nickel towards the hydrogen evolution reaction. *PCCP* **17**, 26864-26874 (2015) <https://doi.org/10.1039/C5CP04238K>

[25] Y. Yuan, N. Yan, P. J. Dyson, Advances in the Rational Design of Rhodium Nanoparticle Catalysts: Control via Manipulation of the Nanoparticle Core and Stabilizer. *ACS Catalysis* **2**, 1057-1069 (2012) <https://doi.org/10.1021/cs300142u>

[26] M. K. Kundu, R. Mishra, T. Bhowmik, S. Barman, Rhodium metal–rhodium oxide (Rh–Rh₂O₃) nanostructures with Pt-like or better activity towards hydrogen evolution and oxidation reactions (HER, HOR) in acid and base: correlating its HOR/HER activity with hydrogen binding energy and oxophilicity of the catalyst. *Journal of Materials Chemistry A* **6**, 23531-23541 (2018) <https://doi.org/10.1039/C8TA07028H>

[27] M. A. Montero, M. R. Gennero de Chialvo, A. C. Chialvo, Kinetics of the hydrogen oxidation reaction on nanostructured rhodium electrodes in alkaline solution. *Journal of Power Sources* **283**, 181-186 (2015) <https://doi.org/10.1016/j.jpowsour.2015.02.133>

[28] D. S. Tran, H. Park, H. Kim, S. K. Kim, Electrodeposited NiRh alloy as an efficient low-precious metal catalyst for alkaline hydrogen oxidation reaction. *International Journal of Energy Research* **45**, 5325-5336 (2021) <https://doi.org/10.1002/er.6155>

[29] P. Benito, V. Dal Santo, V. De Grandi, M. Marelli, G. Fornasari, R. Psaro, A. Vaccari, Coprecipitation versus chemical vapour deposition to prepare Rh/Ni bimetallic catalysts. *Applied Catalysis B: Environmental* **179**, 150-159 (2015) <https://doi.org/10.1016/j.apcatb.2015.05.016>

[30] N. Schiaroli, C. Lucarelli, G. Sanghez de Luna, G. Fornasari, A. Vaccari, Ni-based catalysts to produce synthesis gas by combined reforming of clean biogas. *Applied Catalysis A: General* **582**, 117087 (2019) <https://doi.org/10.1016/j.apcata.2019.05.021>

[31] D. V. Cesar, M. A.S. Baldanza, C. A. Henriques, F. Pompeo, G. Santori, J. Múnera, E. Lombardo, M. Schmal, L. Cornaglia, N. Nichio, Stability of Ni and Rh–Ni catalysts derived from

hydrotalcite-like precursors for the partial oxidation of methane. *International Journal of Hydrogen Energy* **38**, 5616-5626 (2013) <https://doi.org/10.1016/j.ijhydene.2013.02.064>

[32] J. Feng, W. Jiang, C. Yuan, X. Shi, K. Zang, Y. Zhang, Deposition–precipitation approach for preparing core/shell SiO₂@Ni-Rh nanoparticles as an advanced catalyst for the dehydrogenation of 2-methoxycyclohexanol to guaiacol. *Applied Catalysis A: General* **562**, 106-113 (2018) <https://doi.org/10.1016/j.apcata.2018.06.002>

[33] N. A. Nguyen, V. T. Nguyen, S. Shin, H. S. Choi, NiRh nanosponges with highly efficient electrocatalytic performance for hydrogen evolution reaction. *Journal of Alloys and Compounds* **789**, 163-173 (2019) <https://doi.org/10.1016/j.jallcom.2019.03.003>

[34] D. Kutyla, A. Salci, A. Kwecińska, K. Kołczyk-Siedlecka, R. Kowalik, P. Żabiński, R. Solmaz, Catalytic activity of electrodeposited ternary Co–Ni–Rh thin films for water splitting process. *International Journal of Hydrogen Energy* **45**, 34805-34817 (2020) <https://doi.org/10.1016/j.ijhydene.2020.05.196>

[35] C. Carraro, R. Moboudian, L. Magagnin. Metallization and nanostructuring of semiconductor surfaces by galvanic displacement processes. *Surface Science Reports* **62**, 499-525 (2007) DOI: [10.1016/j.surfrep.2007.08.002](https://doi.org/10.1016/j.surfrep.2007.08.002)

[36] I. A. Pasti, N. M. Gavrilov, S. V. Mentus, Electrocatalytic Behavior of Pt/WO₃ Composite Layers Formed Potentiodynamically on Tungsten Surfaces. *Int. J. Electrochem. Sci.* **12**, 5772 – 5791 (2017) DOI: [10.20964/2017.06.80](https://doi.org/10.20964/2017.06.80)

[37] G. Kresse, J. Hafner, Ab initio molecular dynamics for liquid metals. *Phys. Rev. B: Condens. Matter Mater. Phys.* **47**, 558–561 (1993) <https://doi.org/10.1103/PhysRevB.47.558>

[38] G. Kresse, J. Furthmüller, Efficiency of ab-initio total energy calculations for metals and semiconductors using a plane-wave basis set. *Comput. Mater. Sci.* **6**, 15–50 (1996) [https://doi.org/10.1016/0927-0256\(96\)00008-0](https://doi.org/10.1016/0927-0256(96)00008-0)

[39] G. Kresse, J. Furthmüller, Efficient iterative schemes for ab initio total-energy calculations using a plane-wave basis set. *Phys. Rev. B: Condens. Matter Mater. Phys.* **54**, 11169–11186 (1996) DOI: [10.1103/PhysRevB.54.11169](https://doi.org/10.1103/PhysRevB.54.11169)

- [40] J. P. Perdew, K. Burke, M. Ernzerhof, Generalized Gradient Approximation Made Simple. *Phys. Rev. Lett.* **77**, 3865–3868 (1996) <https://doi.org/10.1103/PhysRevLett.77.3865>
- [41] P. E. Blöchl, Projector augmented-wave method. *Phys. Rev. B: Condens. Matter Mater. Phys.* **50**, 17953–17979 (1994) <https://doi.org/10.1103/PhysRevB.50.17953>
- [42] N. Krstajić, M. Popović, B. Grgur, M. Vojnović, D. Šepa, On the kinetics of the hydrogen evolution reaction on nickel in alkaline solution: Part I. The mechanism. *Journal of Electroanalytical Chemistry* **512**, 16-26 (2001) [https://doi.org/10.1016/S0022-0728\(01\)00590-3](https://doi.org/10.1016/S0022-0728(01)00590-3)
- [43] J. K. Norskov, T. Bligaard, A. Logadottir, J. R. Kitchin, J. G. Chen, S. Pandalov, U. Stimming, Trends in the Exchange Current for Hydrogen Evolution. *J. Electrochem. Soc.* **152**, (2005) <https://doi.org/10.1149/1.1856988>
- [44] M. Łukaszewski, M. Soszko, A. Czerwiński, Electrochemical Methods of Real Surface Area Determination of Noble Metal Electrodes – an Overview. *International Journal of Electrochemical Science* **11**, 4442-4469 (2016) DOI: 10.20964/2016.06.71
- [45] S. Trasatti, O. A. Petrii, Real surface area measurements in electrochemistry. *Pure and Applied Chemistry* **63**, 711-734 (1991) <https://doi.org/10.1351/pac199163050711>
- [46] C. C. L. McCrory, S. Jung, I. M. Ferrer, S. M. Chatman, J. C. Peters, T. F. Jaramillo, Benchmarking Hydrogen Evolving Reaction and Oxygen Evolving Reaction Electrocatalysts for Solar Water Splitting Devices. *Journal of the American Chemical Society* **137**, 4347-4357 (2015) DOI: 10.1021/ja510442p
- [47] M. Łukaszewski, H. Siwek, A. Czerwiński, Electrochemical behavior of thin polycrystalline rhodium layers studied by cyclic voltammetry and quartz crystal microbalance. *Electrochimica Acta* **52**, 4560-4565 (2007) <https://doi.org/10.1016/j.electacta.2006.12.066>
- [48] M. Smiljanic, Z. Rakocevic, A. Maksic, S. Strbac, Hydrogen Evolution Reaction on Platinum Catalyzed by Palladium and Rhodium Nanoislands. *Electrochimica Acta* **117**, 336-343 (2014) <https://doi.org/10.1016/j.electacta.2013.11.142>
- [49] M. A. Ehsan, A. Adam, A. Rehman, M. Qamar, Direct Self-Assembly of Hierarchically Grown Rhodium Thin Films for Electrocatalytic Hydrogen Evolution Reaction. *Catalysts* **11**, 338 (2021) <https://doi.org/10.3390/catal11030338>

- [50] S. Fu, J. Song, C. Zhu, G. L. Xu, K. Amine, C. Sun, X. Li, M. H. Engelhard, D. Du, Y. Lin, Ultrafine and highly disordered Ni₂Fe₁ nanofoams enabled highly efficient oxygen evolution reaction in alkaline electrolyte. *Nano Energy* **44**, 319-326 (2018) <https://doi.org/10.1016/j.nanoen.2017.12.010>
- [51] Z. Zhang, Z. H. Lu, H. Tan, X. Chen, Q. Yao, CeO_x-modified RhNi nanoparticles grown on rGO as highly efficient catalysts for complete hydrogen generation from hydrazine borane and hydrazine. *J. Mater. Chem. A* **3**, 23520-23529 (2015) <https://doi.org/10.1039/C5TA06197K>
- [52] Y. Yu, W. Xiao, J. Wang, L. Wang, Understanding the surface segregation behavior of transition metals on Ni(111): a first-principles study. *Phys. Chem. Chem. Phys.* **18**, 26616-26622 (2016) <https://doi.org/10.1039/C6CP02983C>
- [53] W. Sheng, M. Myint, J. G. Chen, Y. Yan, Correlating the hydrogen evolution reaction activity in alkaline electrolytes with the hydrogen binding energy on monometallic surfaces. *Energy Environ. Sci.* **6**, 1509-1512 (2013) <https://doi.org/10.1039/C3EE00045A>
- [54] S. Trasatti, Work function, electronegativity, and electrochemical behaviour of metals: III. Electrolytic hydrogen evolution in acid solutions. *Journal of Electroanalytical Chemistry and Interfacial Electrochemistry* **39**, 163-184 (1972) [https://doi.org/10.1016/S0022-0728\(72\)80485-6](https://doi.org/10.1016/S0022-0728(72)80485-6)
- [55] J. Greeley, T. Jaramillo, J. Bonde, I. Chorkendorff, J. K. Norskov, Computational high-throughput screening of electrocatalytic materials for hydrogen evolution. *Nat. Mater.* **5**, 909-913 (2006) <https://doi.org/10.1038/nmat1752>
- [56] N. Danilovic, R. Subbaraman, D. Strmcnik, K. C. Chang, A. P. Paulikas, V. R. Stamenkovic, N. M. Markovic, Enhancing the Alkaline Hydrogen Evolution Reaction Activity through the Bifunctionality of Ni(OH)₂/Metal Catalysts. *Angew. Chem. Int. Ed.* **51**, 12495-12498 (2012) <https://doi.org/10.1002/anie.201204842>
- [57] A. Michaelides, Z. P. Liu, C. J. Zhang, A. Alavi, D. A. King, P. Hu, Identification of General Linear Relationships between Activation Energies and Enthalpy Changes for Dissociation Reactions at Surfaces. *Journal of the American Chemical Society* **125**, 3704-3705 (2003) DOI: 10.1021/ja027366r
- [58] <https://tradingeconomics.com/commodity/rhodium> (accessed December 14th 2021)

[59] B. Pierozynski, T. Mikolajczyk, I. M. Kowalski, Hydrogen evolution at catalytically-modified nickel foam in alkaline solution. *Journal of Power Sources* **271**, 231-238 (2014)

<https://doi.org/10.1016/j.jpowsour.2014.07.188>

[60] B. J. Plowman, L. A. Jones, S. K. Bhargava, Building with bubbles: the formation of high surface area honeycomb-like films *via* hydrogen bubble templated electrodeposition. *Chem. Commun.* **51**,

4331-4346 (2015) <https://doi.org/10.1039/C4CC06638C>